A Four-Component Decomposition of POLSAR Images Based on the Coherency Matrix

Yoshio Yamaguchi, *Fellow, IEEE*, Yuki Yajima, and Hiroyoshi Yamada, *Member, IEEE*

***Abstract*—A four-component decomposition scheme of the coherency matrix is presented here for the analysis of polarimetric synthetic aperture radar (SAR) images. The coherency matrix is used to deal with nonreflection symmetric scattering case, which is an extension of covariance matrix approach. The same decomposition results have been obtained. The advantage of this approach is explicit expressions of four scattering powers in terms of scattering matrix elements, which serve the interpretation of polarimetric SAR data quantitatively.**

***Index Terms*—Coherency matrix, polarimetric synthetic aperture radar (POLSAR), radar polarimetry, scattering contribution decomposition.**

I. Introduction

TERRAIN and land use classification is one of the most important applications of polarimetric synthetic aperture radar (POLSAR) sensing. A three-component scattering model [1] based on the covariance matrix has been successfully applied to decompose scattering mechanisms in POLSAR image analysis under the reflection symmetry condition $\langle S_{HH}S_{HV}^{*}\rangle = \langle S_{VV}S_{HV}^{*}\rangle = 0$. Following the example of the Freeman three-component decomposition [1], a four-component scattering model [2] has been proposed, which deals with nonreflection symmetric scattering cases $\langle S_{HH}S_{HV}^{*}\rangle \neq 0$ and $\langle S_{VV}S_{HV}^{*}\rangle \neq 0$.

This letter shows a four-component decomposition scheme based on the coherency matrix. Since the information contained in the covariance and coherency matrices is the same, the same decomposition result should be obtained (Fig. 1). However, just a change of polarization basis from the covariance to the coherency matrix does not yield the same expressions for decomposed powers (i.e., for surface scattering power and double-bounce scattering power), because the form of the two matrices is different. Therefore, the purpose of this letter is to show: 1) the four-component decomposition scheme based on the coherency matrix; 2) the equivalence of the decomposed results; and 3) the resultant explicit expressions for decomposed powers in terms of scattering matrix elements, which serve the interpretation of POLSAR data quantitatively.

This letter is organized as follows. In Section II we introduce the coherency matrix and its modeling, and in Section III we define the four matrices corresponding to some elementary scattering models. In Section IV, the four-component scattering powers are derived in terms of the scattering matrix elements, and in Section V, L-band Pi-SAR data are used to illustrate the equivalence of the coherency matrix approach and the covariance matrix approach.

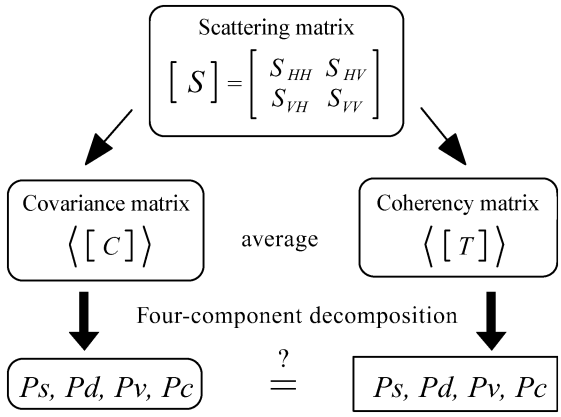

Fig. 1. Four-component decomposition using covariance and coherency matrices.

II. Coherency Matrix

To derive polarimetric scattering characteristics in a POLSAR image, it is necessary to evaluate the second-order statistics of scattering matrix. Here, we focus on a 3×3 coherency matrix based on the mathematically orthogonal Pauli matrices [3]. The ensemble average coherency matrix can be expressed in terms of scattering matrix elements as in (1), shown at the bottom of the next page, where $\langle\rangle$ denotes ensemble average in the data processing. For mathematical modeling for decomposition, we need to derive basis matrices corresponding to volume, surface, double bounce, and helix scattering components [2]. The first step is to derive the mathematical average of the coherency matrix.

For simplicity, we start with the scattering matrix and write it as

$$[S(HV)] = \begin{bmatrix} S_{HH} & S_{HV} \\ S_{VH} & S_{VV} \end{bmatrix} = \begin{bmatrix} a & c \\ c & b \end{bmatrix} \tag{2}$$

assuming the backscattering case $S_{HV} = S_{VH} = c$. We do not neglect the cross-component term S_{HV} so that we can deal with general case. Then, its rotation by angle θ around the radar line of sight leads to

$$[S(hv)] = \begin{bmatrix} S_{hh} & S_{hv} \\ S_{vh} & S_{vv} \end{bmatrix} = \begin{bmatrix} \cos\theta & \sin\theta \\ -\sin\theta & \cos\theta \end{bmatrix} \begin{bmatrix} S_{HH} & S_{HV} \\ S_{VH} & S_{VV} \end{bmatrix} \begin{bmatrix} \cos\theta & -\sin\theta \\ \sin\theta & \cos\theta \end{bmatrix} \tag{3}$$

Manuscript received August 7, 2005; revised October 28, 2005. This work in part was supported by Grant in Aid for Scientific Research and Toyota Central R&D Labs. The work is also carried out in cooperation with Center for Information and Communications Research, Niigata University.

The authors are with the Faculty of Engineering, Niigata University, Nigata 950-2181, Japan (e-mail: yamaguch@ie.niigata-u.ac.jp).

Digital Object Identifier 10.1109/LGRS.2006.869986

where the capital letters HV refer to the original coordinate and also the actually measured quantities, and the hv refers to the rotated coordinate and is used in the mathematical formulation. There is a difference between HV and hv. $\langle[T]\rangle^{HV}$ indicates spatial ensemble averaging of the measured data, whereas $\langle[T]\rangle^{hv}$ corresponds to mathematical averaging obtained here by integration.

The mathematical form of averaging with probability density function $p(\theta)$ is given by

$$\langle S_{hv}\, S_{hv}^{*}\rangle = \int_{0}^{2\pi} S_{hv} S_{hv}^{*} p(\theta) d\theta. \tag{4}$$

If the probability density function is assumed to be uniform $p(\theta) = 1/(2\pi)$, then the integration can be carried out easily for all combinations of scattering matrix elements [2]. The mathematical averaging of the coherency matrix becomes

$$\langle[T]\rangle^{hv} = \begin{bmatrix} \frac{1}{2}|a+b|^2 & 0 & 0 \\ 0 & \frac{1}{4}|a-b|^2+|c|^2 & j\mathrm{Im}\{c^*(a-b)\} \\ 0 & -j\mathrm{Im}\{c^*(a-b)\} & \frac{1}{4}|a-b|^2+|c|^2 \end{bmatrix}. \tag{5}$$

The eigenvalues, the anisotropy A, as well as the total power may be derived directly from (5) for this uniform distribution case

$$\lambda_1 = \frac{1}{2}|a+b|^2 \tag{6a}$$

$$\lambda_2 = \frac{1}{4}|a-b|^2 + |c|^2 + \mathrm{Im}\{c^*(a-b)\} \tag{6b}$$

$$\lambda_3 = \frac{1}{4}|a-b|^2 + |c|^2 - \mathrm{Im}\{c^*(a-b)\} \tag{6c}$$

$$\text{Total power} = \lambda_1 + \lambda_2 + \lambda_3 = \mathrm{Tr}\langle[T]\rangle^{hv} \tag{6d}$$

$$A = \frac{\lambda_2' - \lambda_3'}{\lambda_2' + \lambda_3'},\ with\ \lambda_1' > \lambda_2' > \lambda_3' \quad (\lambda_1', \lambda_2', \lambda_3') \subseteq (\lambda_1, \lambda_2, \lambda_3). \tag{6e}$$

III. Basis Coherency Matrices for the Four-Scattering Model

The next step is to choose basis coherency matrices which represent surface, double bounce, volume, and helix scattering. Keeping in mind the forms of (1) and (5) and the four-component decomposition model in the covariance matrix case [2], we take the following basis coherency matrices. The concept of helix mechanism has been mainly developed by Krogager for his sphere, deplane, helix coherent decomposition [4].

For the helix scattering model, we take a helix scattering matrix, so that

$$[S]_{r-\mathrm{helix}}^{HV} = \frac{e^{j2\theta}}{2}\begin{bmatrix} 1 & -j \\ -j & -1 \end{bmatrix}$$

$$\Rightarrow \langle[T]\rangle_{r-\mathrm{helix}}^{hv} = \frac{1}{2}\begin{bmatrix} 0 & 0 & 0 \\ 0 & 1 & j \\ 0 & -j & 1 \end{bmatrix} \tag{7a}$$

$$[S]_{l-\mathrm{helix}}^{HV} = \frac{e^{-j2\theta}}{2}\begin{bmatrix} 1 & j \\ j & -1 \end{bmatrix}$$

$$\Rightarrow \langle[T]\rangle_{l-\mathrm{helix}}^{hv} = \frac{1}{2}\begin{bmatrix} 0 & 0 & 0 \\ 0 & 1 & -j \\ 0 & j & 1 \end{bmatrix}. \tag{7b}$$

This matrix is responsible for the term $\mathrm{Im}\{c^*(a-b)\}$ in (5) which has been neglected for the three-component scattering model [1] under the reflection symmetry condition $\langle S_{HH} S_{HV}^{*}\rangle = \langle S_{VV} S_{HV}^{*}\rangle = 0$.

For the volume scattering, we employ a randomly oriented dipole model. The corresponding coherency matrix is

$$[S]^{HV} = \begin{bmatrix} 1 & 0 \\ 0 & 0 \end{bmatrix} \text{ or } [S]^{HV} = \begin{bmatrix} 0 & 0 \\ 0 & 1 \end{bmatrix}$$

$$\Rightarrow \langle[T]\rangle_{\mathrm{vol}}^{hv} = \frac{1}{4}\begin{bmatrix} 2 & 0 & 0 \\ 0 & 1 & 0 \\ 0 & 0 & 1 \end{bmatrix}. \tag{8}$$

The single-bounce model is represented by surface scattering phenomena from slightly rough surface in which the cross-polarized component is negligible. The scattering matrix for a Bragg surface has the form

$$[S]^{HV} = \begin{bmatrix} R_h & 0 \\ 0 & R_v \end{bmatrix}. \tag{9}$$

The reflection coefficients for horizontally and vertically polarized waves are given by [5]

$$R_h = \frac{\cos\theta - \sqrt{\varepsilon_r - \sin^2\theta}}{\cos\theta + \sqrt{\varepsilon_r - \sin^2\theta}}$$

$$R_v = \frac{(\varepsilon_r - 1)\left\{\sin^2\theta - \varepsilon_r(1+\sin^2\theta)\right\}}{(\varepsilon_r \cos\theta + \sqrt{\varepsilon_r - \sin^2\theta})^2} \tag{10}$$

$$\langle[T]\rangle^{HV} = \begin{bmatrix} \frac{1}{2}\left\langle|S_{HH}+S_{VV}|^2\right\rangle & \frac{1}{2}\left\langle(S_{HH}+S_{VV})(S_{HH}-S_{VV})^*\right\rangle & \left\langle(S_{HH}+S_{VV})S_{HV}^*\right\rangle \\ \frac{1}{2}\left\langle(S_{HH}-S_{VV})(S_{HH}+S_{VV})^*\right\rangle & \frac{1}{2}\left\langle|S_{HH}-S_{VV}|^2\right\rangle & \left\langle(S_{HH}-S_{VV})S_{HV}^*\right\rangle \\ \left\langle S_{HV}(S_{HH}+S_{VV})^*\right\rangle & \left\langle S_{HV}(S_{HH}-S_{VV})^*\right\rangle & \left\langle 2|S_{HV}|^2\right\rangle \end{bmatrix} \tag{1}$$

where θ is the incidence angle, and ε_r is the relative dielectric constant of the surface. This scattering matrix yields a surface scattering coherency matrix as

$$[T]^{hv}_{\text{surface}} = \begin{bmatrix} 1 & \beta^* & 0 \\ \beta & |\beta|^2 & 0 \\ 0 & 0 & 0 \end{bmatrix} \quad \text{with} \quad \beta = \frac{R_h - R_v}{R_h + R_v}. \tag{11}$$

We can assume $|\beta| < 0.5$ for normal radar observation of land surfaces.

The double-bounce model is based on the hypothesis of double reflections from right angle structures. Assuming $|a+b| < |a-b|$ in the scattering matrix (2), we define $\alpha = (a+b)/(a-b)$ with $|\alpha| < 1$. In this case, the coherency matrix for double-bounce scattering can be written as

$$[T]^{hv}_{\text{double}} = \begin{bmatrix} |\alpha|^2 & \alpha & 0 \\ \alpha^* & 1 & 0 \\ 0 & 0 & 0 \end{bmatrix}. \tag{12}$$

IV. Four-Component Decomposition by the Coherency Matrix

Using the four components (7), (8), (11), and (12), we expand the measured coherency matrix as

$$\langle [T] \rangle^{HV} = f_s [T]^{hv}_{\text{surface}} + f_d [T]^{hv}_{\text{double}} + f_v \langle [T] \rangle^{hv}_{\text{vol}} + f_c \langle [T] \rangle^{hv}_{\text{helix}} \tag{13}$$

$$= f_s \begin{bmatrix} 1 & \beta^* & 0 \\ \beta & |\beta|^2 & 0 \\ 0 & 0 & 0 \end{bmatrix} + f_d \begin{bmatrix} |\alpha|^2 & \alpha & 0 \\ \alpha^* & 1 & 0 \\ 0 & 0 & 0 \end{bmatrix} + \frac{f_v}{4} \begin{bmatrix} 2 & 0 & 0 \\ 0 & 1 & 0 \\ 0 & 0 & 1 \end{bmatrix} + \frac{f_c}{2} \begin{bmatrix} 0 & 0 & 0 \\ 0 & 1 & \pm j \\ 0 & \pm j & 1 \end{bmatrix} \tag{14}$$

where f_s, f_d, f_v, and f_c are the expansion coefficients to be determined. Now comparing the coherency matrix elements, we have the following five equations with six unknowns α, β, f_s, f_d, f_v, and f_c:

$$|\text{Im}\langle S^*_{HV}(S_{HH} - S_{VV})\rangle| = \frac{f_c}{2} \tag{15a}$$

$$\langle 2|S_{HV}|^2 \rangle = \frac{f_v}{4} + \frac{f_c}{2} \tag{15b}$$

$$\frac{1}{2}\langle |S_{HH} - S_{VV}|^2 \rangle = f_s|\beta|^2 + f_d + \frac{f_v}{4} + \frac{f_c}{2} \tag{15c}$$

$$\frac{1}{2}\langle |S_{HH} + S_{VV}|^2 \rangle = f_s + f_d|\alpha|^2 + \frac{f_v}{4} \tag{15d}$$

$$\frac{1}{2}\langle (S_{HH} + S_{VV})(S_{HH} - S_{VV})^* \rangle = f_s\beta^* + f_d\alpha. \tag{15e}$$

Since the left-hand sides of (15) are measurable quantities, we can determine f_c directly by (15a)

$$f_c = 2\,|\text{Im}\langle S^*_{HV}(S_{HH} - S_{VV})\rangle|. \tag{16}$$

The sense of rotation is determined by the sign of (16) referring to (7), so that we have the following:

Right-circular polarization:

$$\text{Im}\langle S^*_{HV}(S_{HH} - S_{VV})\rangle > 0 \tag{17a}$$

Left-circular polarization:

$$\text{Im}\langle S^*_{HV}(S_{HH} - S_{VV})\rangle < 0. \tag{17b}$$

Then (15b) gives the volume scattering coefficient directly as

$$f_v = 8\langle |S_{HV}|^2 \rangle - 4\,|\text{Im}\langle S^*_{HV}(S_{HH} - S_{VV})\rangle|. \tag{18}$$

The remaining four unknowns with three equations can be obtained as follows. If $\text{Re}\langle S_{HH}S^*_{VV}\rangle > 0$ in the area of interest, we regard $\alpha = 0$ (zero double bounce) in this area because $\text{Re}\langle S_{HH}S^*_{VV}\rangle > 0$ indicates that surface scattering is dominant. Then the unknowns are determined by

$$f_s = B \quad \beta^* = \frac{C}{B} \quad f_d = A - \frac{|C|^2}{B}. \tag{19}$$

If $\text{Re}\langle S_{HH}S^*_{VV}\rangle < 0$, then $\beta^* = 0$. Since $\text{Re}\langle S_{HH}S^*_{VV}\rangle < 0$ is an indicator for double-bounce occurrence, we can consider the surface scattering as negligible and derive

$$f_d = A \quad \alpha = \frac{C}{A} \quad f_s = B - \frac{|C|^2}{A} \tag{20}$$

where A, B, and C are given by

$$A = \frac{1}{2}\langle |S_{HH} - S_{VV}|^2 \rangle - 2\langle |S_{HV}|^2 \rangle \tag{21a}$$

$$B = \frac{1}{2}\langle |S_{HH} + S_{VV}|^2 \rangle - 4\langle |S_{HV}|^2 \rangle + 2\,|\text{Im}\langle S^*_{HV}(S_{HH} - S_{VV})\rangle| \tag{21b}$$

$$C = \frac{1}{2}\langle (S_{HH} + S_{VV})(S_{HH} - S_{VV}|^* \rangle. \tag{21c}$$

Finally, the scattering powers Ps, Pd, Pv, and Pc corresponding to surface, double bounce, volume, and helix scattering, respectively, are determined by

$$P_s = f_s\left(1 + |\beta|^2\right) \quad P_d = f_d\left(1 + |\alpha|^2\right) \quad P_v = f_v \quad P_c = f_c. \tag{22}$$

The powers Pc and Pv have exactly the same form derived by covariance matrix approach [2]. Therefore the equivalence is guaranteed. As regards to Ps and Pd, we can check the validity by means of the following considerations. To a reasonable degree in the coherency matrix, the term $\langle |S_{HH} + S_{VV}|^2 \rangle/2$ represents single-bounce power, and the term $\langle |S_{HH} - S_{VV}|^2 \rangle/2$ corresponds to double-bounce power. The detailed examination of (19)–(22) shows that these interpretations are true, but they are slightly modified according to (19)–(22) for the nonreflection symmetry case. For quantitative evaluation, we need to compare these with actual data as it will be done in the following section.

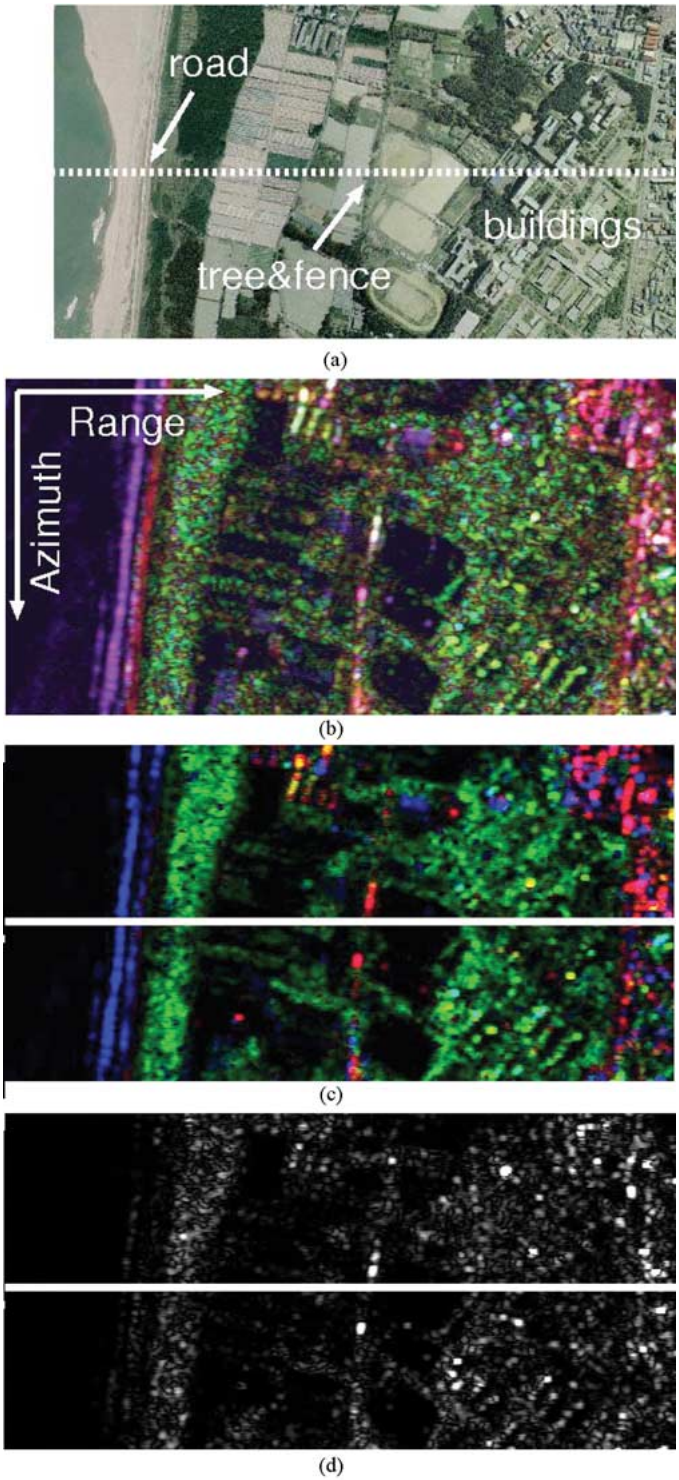

Fig. 2. Polarimetric image near Niigata University. (a) Aerial photo. (b) HH (red), VV (blue), and HV (green). (c) Pd (red), Ps (blue), Pv (green). (d) Pc (grayscale). The dotted transect in (a) corresponds to the transect (c).

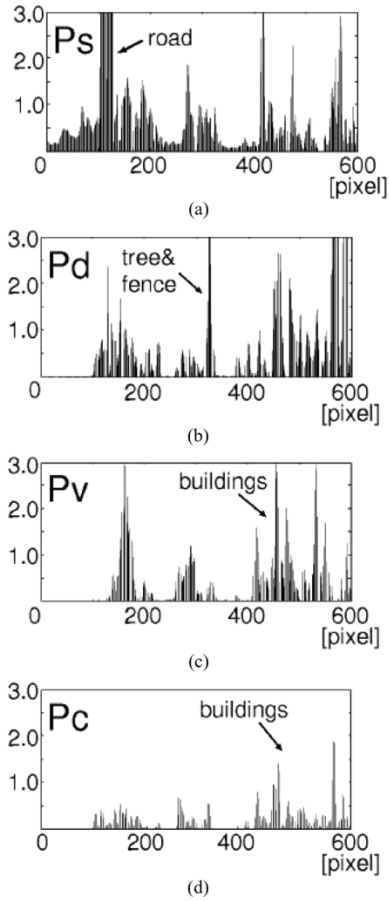

Fig. 3. Four-component decomposition results. (a) Surface scattering power Ps along a transect in Fig. 2(c). (b) Double-bounce scattering power Pd. (c) Volume scattering power Pv. (d) Helix scattering power Pc along a transect in Fig. 2(d).

V. Decomposition Example and Comparison With Covariance Matrix Approach

The decomposition scheme was applied to various L-band Pi-SAR datasets. The area chosen is that of the Niigata University, Japan, which includes sea, pine trees, crop fields, a baseball ground, and buildings as shown in Fig. 2(a). Fig. 2(b) shows a polarimetric color composite image with HH (red), HV (green), and VV (blue). Also the decomposed power images by the coherency matrix are shown in Fig. 2(c) with Ps (blue), Pd (red), and Pv (green) and in Fig. 2(d) with Pc (grayscale). Since Pc and Pv are exactly of the same form as in the model derived by the covariance matrix, we paid more attention to the remaining surface scattering power Ps, and double-bounce scattering power Pd. For quantitative comparison, we chose a transect in Fig. 2(c) and (d), and compared the resultant powers by both methods. The dotted transect in Fig. 2(a) corresponds to the transect in Fig. 2(c). Fig. 3(a) shows the magnitude Ps along the transect. Since the power plot derived by the coherency matrix approach coincided with that of the covariance matrix approach, only one plot was shown in Fig. 3(a) instead of both plots. Fig. 3(b) shows the case for double-bounce scattering Pd along the transect, which also results in exactly the same pattern for both methods. Fig. 3(c) and (d) corresponds to the volume scattering power Pv and helix scattering power Pc. We can observe some peaks in Fig. 3 which are caused by corresponding targets shown in the aerial photo Fig. 2(a). For example, the "road boundary" in Fig. 2(a) is strong for Ps; "tree & fence" appears for Pd; and Pc increases in regions with building. These power decompositions correspond to actual scattering phenomena and verify this approach.

VI. Concluding Remarks

It is shown that the four-component decomposition results based on the coherency matrix are identical to those based on the covariance matrix. Although the expansion matrix is different, the same result has been obtained. Since the scattering powers can be expressed explicitly by the coherent matrix approach, this decomposition has advantages in the interpretation of SAR scattering mechanism in terms of scattering element and in its implementation. The expansion method should be further developed for special scattering scenarios where (21a) and (21b) become negative.

Acknowledgment

The authors are grateful to the Japan National Institute of Information and Communications Technology and the Japan Aerospace Exploration Agency for providing the Pi-SAR data.

References

[1] A. Freeman and S. L. Durden, "A three-component scattering model for polarimetric SAR data," *IEEE Trans. Geosci. Remote Sens.*, vol. 36, no. 3, pp. 936–973, May 1998.

[2] Y. Yamaguchi, T. Moriyama, M. Ishido, and H. Yamada, "Four-component scattering model for polarimetric SAR image decomposition," *IEEE Trans. Geosci. Remote Sens.*, vol. 43, no. 8, pp. 1699–1706, Aug. 2005.

[3] S. R. Cloude and E. Pottier, "A review of target decomposition theorems in radar polarimetry," *IEEE Trans. Geosci. Remote Sens.*, vol. 34, no. 2, pp. 498–518, Mar. 1996.

[4] E. Krogager, "Aspects of polarimetric radar imaging," Ph.D. dissertation, Danish Def. Res. Est., Copenhagen, 1993.

[5] Y. Oh, K. Sarabandi, and F. T. Ulaby, "An empirical model and an inversion technique for radar scattering from bare soil surfaces," *IEEE Trans. Geosci. Remote Sens.*, vol. 30, no. 2, pp. 370–381, Mar. 1992.